Nanostructured photon management for high performance solar cells

Jia Zhu, Zongfu Yu, Shanhui Fan, Yi Cui *

Department of Materials Science and Engineering, Stanford University, 476 Lomita Mall, McCullough Building 343, Stanford, CA 94305, USA

ABSTRACT

Advanced photon management, involving both absorption enhancement and reflection reduction, is critical to all photovoltaic devices. Here we discuss a novel solar cell structure with an efficient photon management design. The centerpiece of the design is the nanocone structure, which is fabricated by a scalable low temperature process. With this design, devices with a very thin active layer can achieve near perfect absorption because of both efficient anti-reflection and absorption enhancement over a broadband of spectra and a wide range of angles of incidence. The device performance of this design is significantly superior to that of conventional devices. More excitingly, the design and process is in principle not limited to any specific materials; hence it opens up exciting opportunities for a variety of photovoltaic devices to further improve the performance, reduce materials usage, and relieve the abundance limitation.

© 2010 Elsevier B.V. All rights reserved.

Contents

1. Introduction

The increased concern about detrimental long-term effects of emission of CO_2 and other greenhouse gases and the decreased availability of fossil fuel sources are driving tremendous research efforts for renewable energy technologies. Solar cells, which harvest energy directly from sunlight and convert it into electricity, are widely recognized as an essential component of the future energy supply. In spite of a substantial drop in module cost in the past several decades, significant technology improvements in both device performance and the manufacturing process are still necessary for photovoltaics to be economically competitive for terawatt-scale applications.

Currently photovoltaic production is dominated by crystalline silicon modules, which represent about 90% of the market. Around half of the cost of c-Si modules is from the silicon wafers. Even though module cost is recently decreasing substantially as the production rate is increasing, it is estimated that costs for wafer based Si modules will be in the range of $1–1.5/$W_p$ in the next 10 years, significantly higher than $0.33/$W_p$ target set by U.S. Department of Energy for utility scale applications. Therefore, there has been a significant effort over the past decade in the

development of thin-film solar cells [1] that do not require the use of silicon wafers and therefore can be manufactured at much reduced cost. Unlike wafers, with their 200–300 μm thicknesses, thin-film solar cells have thickness typically in the range of 1–2 μm, deposited on cheap substrates such as glass or stainless steel. Currently, there are three leading thin-film technologies, cadmium telluride (CdTe), copper indium diselenide ($CuInSe_2$), and hydrogenated amorphous silicon (a-Si:H) [2,3]. While thin-film solar cells, notably, CdTe modules from First Solar, have demonstrated significant cost reduction, with a compelling low manufacturing cost of $1/W_p$, there is still much room for further improvement. Typically, efficiencies achieved in the lab are much lower than the theoretical limit, due to both optical and electrical losses. The large capital cost calls for the development of high throughput processes. Probably one of the biggest concerns regarding thin-film solar cells of CdTe and $CuInSe_2$ is their usage of scarce elements like tellurium and indium, which will fundamentally limit their scales of applications.

For both performance improvement and cost reduction, photon management is critical to the development of next generation photovoltaic devices. It is an essential component to boost the efficiency towards the theoretical limit, since it can not only minimize optical losses, including inefficient absorption near the bandgap and reflection at the interfaces, but it also could reduce transport losses due to shortened carrier collection length. By enabling efficient light absorption within much thinner materials, photon management design is also critical for manufacturing cost reduction, since it can greatly reduce film thickness, improve the throughput, and expand the range and quality of materials. For CdTe and $CuInSe_2$, the benefit of the implementation of photon management design is more significant since their ultimate application scales will be expanded through reduced usage of scarce elements.

However, efficient photon management design is rather challenging, primarily due to the broadband nature of the solar spectrum and cost restrictions of module fabrication. An examination of current photovoltaic technologies reveals that the photon management designs vary greatly a lot for different kinds of devices. For c-Si solar cells, a representative example is illustrated in Fig. 1, known as the "PERL" structure [4]. Even though the development of the "PERL" structure involves lithography, which largely limits the exact structure from large-scale applications, the structure is a classical demonstration of light trapping in c-Si solar cells. An inverted pyramid surface and double layer anti-reflection coatings are the main features for the light-trapping scheme. The inverted pyramid arrays have two main functions. First, they allow light to reflect multiple times before escaping, which minimizes the reflection loss to a large extent. Second, they refract light into large angles, thereby dramatically increasing the optical path
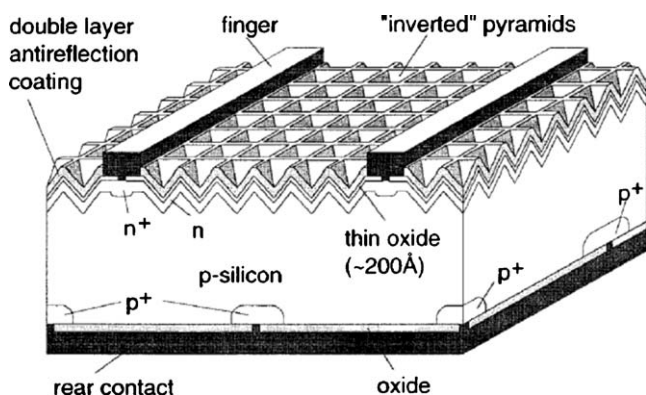

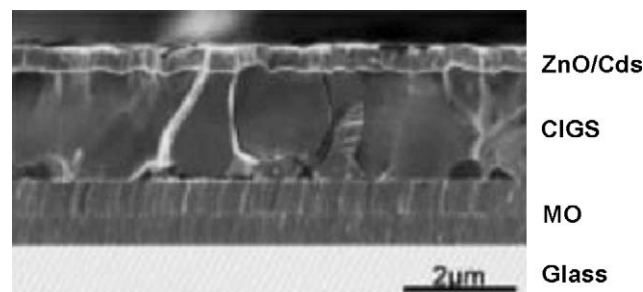**Fig. 2.** (Ref. [34]) Cross-sectional scanning electron microscopy images of a Cu(InGa)Se₂ (CIGS) solar cell.

length. For these two functions to work properly, the feature sizes of these pyramid arrays are typically around tens of microns, significantly larger than the wavelength of the utilized solar spectrum (Fig. 2).

For thin-film solar cells with absorbers only around 1–2 μm thick, the pyramid design is not feasible. In such cells, a quarter wavelength of transparent conducting oxide is typically used as an anti-reflection coating, and a layer of highly reflective metal, such as silver or aluminum, is used as a rear surface mirror to enhance the absorption. In some cases, like a-Si:H solar cells, a thin layer of randomly textured transparent conducting oxide (aluminum doped zinc oxide as an example) is used to scatter the light to further enhance the optical path. However, the quarter wavelength anti-reflection layer works efficiently only within a narrow range of wavelengths. The absorption enhancement effects of random textured oxide obtained to date are far from optimal, calling for a better understanding and further technological improvement of photon management in the sub-wavelength regime.

The ideal photon management design for the next generation solar cells should work for a broad range of the spectrum with a feature size in the sub-wavelength regime, and it must be achievable at very large scale. Nanostructures, with a scale comparable to the wavelengths of most of the utilized solar spectrum, enable an unprecedented manipulation of the flow of photons; therefore, they are widely considered as promising candidates for the advanced photon management design. A variety of nanostructure based photon management designs have been proposed and extensively pursued recently. For example, a significant amount of nanophotonic structures have been reported in the literature for both fundamental understanding and novel applications, including photonic crystals, metamaterials [5], and plasmonics [6,7]. However, this review article will focus on nanostructure based photon management designs specifically for photovoltaic applications, with essentially two functions: suppressing reflection and enhancing absorption across a broad range of the solar spectrum. Plasmonic solar cells, a new type of solar cells which use the scattering from noble metal nanoparticles excited at their surface plasmon resonance, will only be briefly mentioned. Interested readers are directed to other sources for further information [8–15].

2. Fabrication of nanowire and nanocone arrays

The tailoring of morphologies is an essential requirement for any nanostructures to efficiently manipulate the flow of photons. Various parameters such as shapes, diameters, and spacings of these nanostructures must be well controlled across a wide range, and be achieved in a large scale. With rapid development of nanotechnology over the past decade, a handful of methods have been developed to fabricate nanostructures in a large scale. For example, vapor–liquid–solid method has been used to synthesize nanowire arrays with high diameter control; however, it is very

Fig. 1. (Ref. [4]) PERL (passivated emitter, rear locally diffused) cell structure.

challenging to control spacings between nanowires. Solution chemistry is an alternative for synthesis of nanowire arrays, although the control of both spacing and diameter is limited. Electron-beam and photolithography have a very good controllability of feature size down to 100 nm or even smaller, but the cost is high and the throughput is low, not feasible for large-scale applications. Few processes developed so far can fabricate nanostructures with a fine control of shapes, diameters and spacings in a large scale. Nanosphere lithography, which combines colloidal nanoparticle synthesis and state of art fabrication techniques, is one of the most promising ways to achieve this goal [16,17].

2.1. Method

Recently, by combining Langmuir–Blodgett (LB) assembly with reactive ion etching (RIE), we have developed a large scale and low temperature process to fabricate nanostructures. It provides precise control of diameters, spacings and shapes across a wide range, from tens of nanometers to several microns [18,19]. Even though only Si is used for the demonstration of the concept, the process can be applied to a large variety of materials. Fig. 3 shows the general fabrication process. Monodisperse SiO_2 nanoparticles, synthesized in-house, are assembled into a close-packed monolayer on top of a silicon wafer using the LB method. Monodisperse SiO_2 particles, with diameters from 50 to 800 nm, are produced by a modified Stöber synthesis. The particles are modified with aminopropyldiethoxymethylsilane so as to terminate them with positively charged amine groups, preventing aggregation. The diameter and spacing of the nanoparticles can be further tuned by selective and isotropic RIE of SiO_2 (Fig. 3(b)). The RIE etching is based on fluorine chemistry, using a mixture of O_2 and CHF_3. Si nanowires and nanocones can similarly be obtained by using Cl_2 based selective and anisotropic RIE (Fig. 3(c)). The diameter and spacing of these nanostructures are determined by the initial nanoparticle sizes and both SiO_2 and Si etching times. SiO_2 particles can be removed by hydrofluoric acid (HF), if needed (Fig. 3(d)).

2.2. Shape control: nanowires and nanocones

One unique advantage of our process is the control over the shape. Depending on the conditions of RIE, either nanowire or nanocone can be obtained. There are several mechanisms behind the formation of nanocones. First, Cl and Br free radicals arrive at the Si surface from all directions during RIE, inducing some
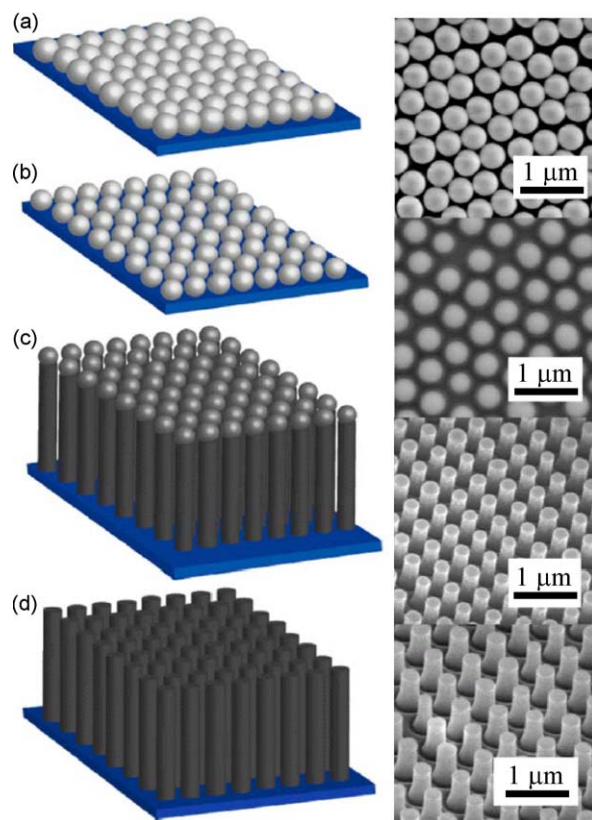

Fig. 3. Fabrication process of nanowires.

isotropic etching of Si or undercutting during the supposedly anisotropic steps. Second, the etching selectivity of Si to SiO_2 is around 26; therefore, the extent of lateral etching will increase due to mask erosion when using SiO_2 masks. Last, tapered sidewalls can occur when the etched products are redeposited during etching, since the redeposition rate decreases from the bottom to the top of the pillar.

With the understanding of formation mechanisms, the undercutting can be utilized to form uniquely sharp nanocones through control of the etching conditions. The aspect ratio and the tip radius of these nanocones can be precisely controlled. First, Si nanowires are formed by Cl_2 based anisotropic RIE. Second, C_2ClF_5/SF_6 is used for further isotropic etching of preformed nanowires,
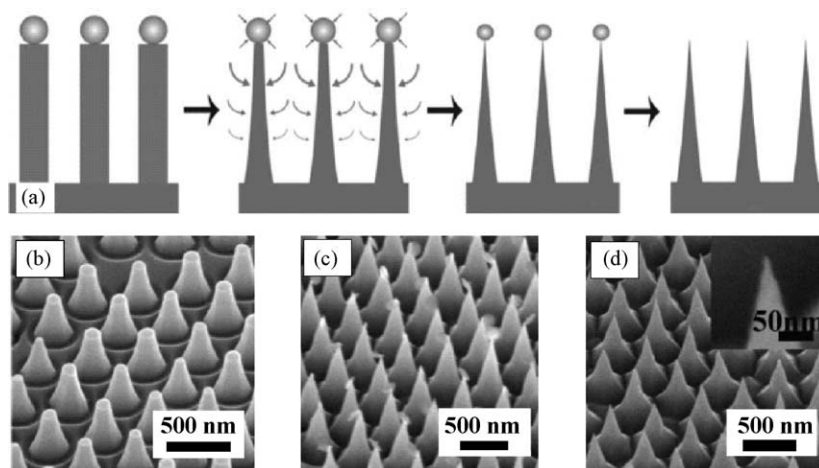

Fig. 4. Schematic of sharpening process with thicker arrows indicating faster etching rate.
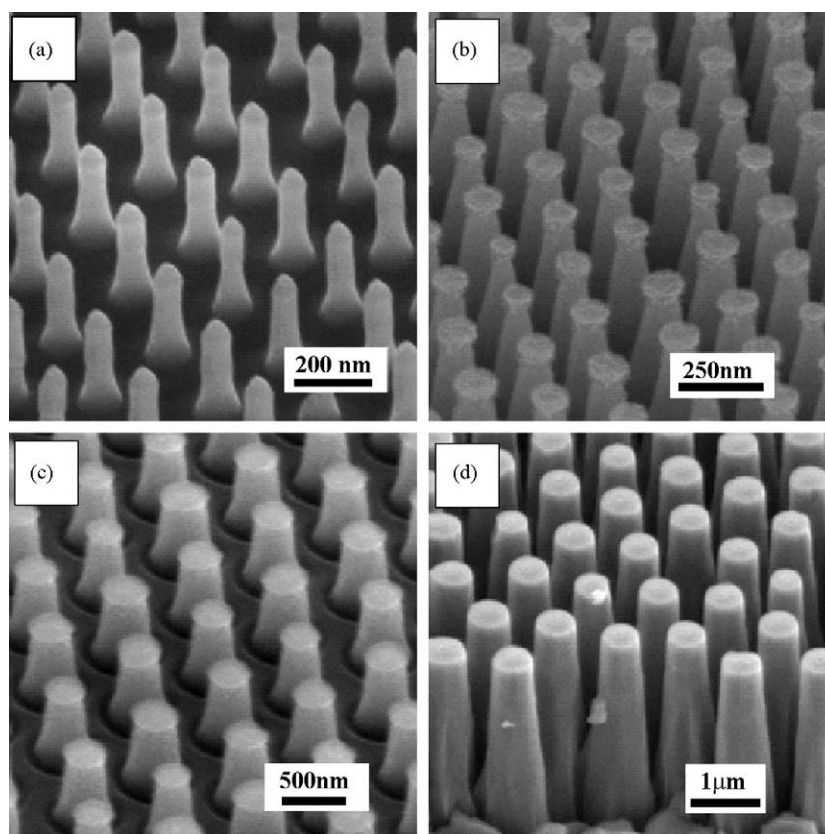
Fig. 5. SEM images of nanowire arrays with uniform diameter of (a) 60, (b) 125, (c) 300, and (d) 600 nm.

which creates undercut and sharpens the nanowires (Fig. 4(a)). Fig. 4(b)–(d) shows the SEM images at different stages of the sharpening process. Accompanying the sharpening is the shrinkage of SiO_2 spheres. The combination of anisotropic and isotropic etching can lead to a sharpening of the tips to a radius of curvature of 5 nm, opening up the opportunities for refractive index matching, which will be explained in detail in section III.

2.3. Diameter and spacing control

Besides the shapes of these nanowire and nanocone arrays, the diameter (D) and spacing (S) can also be rationally designed. Since the center-to-center distance of neighboring nanostructures is $D + S$, the SiO_2 nanoparticles can be chosen to have an initial diameter of $D + S$ and to be etched by $S/2$. The diameter of the initial SiO_2 nanoparticles can be precisely controlled from 50 nm to 1 μm during the synthesis. RIE etching can be controlled with an accuracy of ∼10 nm. Thus, we have precise control of diameter and spacing over a wide range. Figs. 5 and 6 give two examples of fine control of diameter and spacing correspondingly. Fig. 5 shows the nanowires with desired diameters between 60 and 600 nm. Fig. 6 shows the nanowires with desired spacing between 50 and 400 nm.

2.4. Large-scale process

Another important characteristic of our process is that it can be applied to a large scale. As explained above, the scale achievable in our process is essentially defined by the area of SiO_2 particles' coverage. We have demonstrated that close-packed monolayers of nanoparticles can be produced on a wafer-scale with a reasonable throughput. Fig. 7 shows a photograph of a 4-in. wafer covered uniformly by a monolayer of 200 nm diameter SiO_2 particles.

Scanning electron microscope (SEM) images at four randomly picked locations far from each other show that a monolayer of particles covers the whole wafer.

3. Photon management: anti-reflection

When light hits the interface between media characterized by different refractive indices, a significant fraction of it is reflected. For example, without any treatment, around 30% of light would be lost due to reflection at the interface of between air and Si. Therefore, reflection is a serious problem not only for solar cells but also for many other optoelectronic devices, such as light-emitting diodes (LED) [20–22] and photo detectors. A range of techniques has been developed to reduce reflection for different applications [20,22]. Now, the industrial standard of anti-reflection coating for thin-film solar cells is to use a quarter wavelength transparent layer with destructive interference. However, this technique only works for a narrow range of wavelengths.

3.1. Nanowires

Over the past few years, nanostructures have been heavily investigated for broadband reflection suppression. Nanowires arrays with moderate filling ratio were found to be able to greatly reduce reflectance [19,23–26], since they essentially provide an intermediate refractive index step (Fig. 8(b)). An even more ideal anti-reflection technique is to provide impedance matching through a gradual reduction of the effective refractive index (Fig. 8(c)). With graded-refractive index layers, light only experiences a gradual change of the refractive index instead of hitting a sharp interface (see Fig. 2(a)), and reflection can be efficiently eliminated for a large range of wavelengths and angles of incidence.
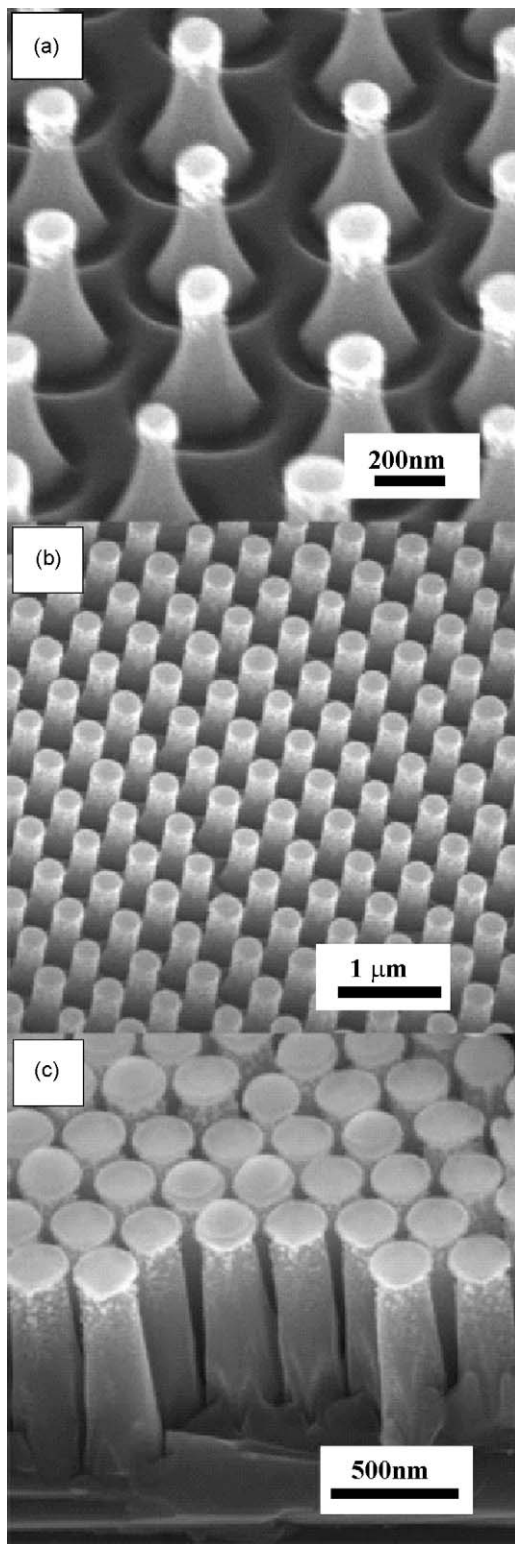
Fig. 6. Nanowire arrays with a spacing of (a) 400, (b) 350, and (c) 50 nm.

One example of nanowire based graded-refractive index design is shown in Fig. 9. Several layers of nanowire arrays of different materials, densities and tilting angles are carefully designed and deposited in sequence to form a graded-index coating [27]. It was found that the reflection can be suppressed down to 0.5% for a broad range of wavelengths and angles of incidence.

3.2. Nanocones

Nanocone arrays with a gradual change of diameter from the bottom to the top can provide another version of graded-index coating [19,28], which has an efficient broadband anti-reflection property and great processing advantages. We have performed an experiment to evaluate the anti-reflection effect of nanowires and nanocones, as compared to thin film. Three samples were fabricated, with a 1 μm-thick a-Si:H thin film deposited onto each. A monolayer of silica nanoparticles was preformed on the second and third samples. After RIE etching, nanowire and nanocone arrays were formed on the second and third samples, respectively because of different etching conditions as explained in section II. Fig. 10 (left) shows a SEM image of an a-Si:H nanowire array after RIE. The dimensions of each nanowire were ∼300 nm wide by ∼600 nm long. The silica nanoparticles can still clearly be seen on the top of each nanowire. Fig. 10 (right) shows a SEM image of an a-Si:H nanocone array. Each nanocone was also ∼600 nm long. The tip diameter of these nanocones was ∼20 nm, while the base diameter was ∼300 nm. After RIE, the silica nanoparticles were so small that they were no longer observable on top of the NCs.

Fig. 11 shows a photograph of these three samples. The thin-film sample had a highly reflective, mirror-like surface (Fig. 11 left). The sample with a nanowire array reflected less light (Fig. 11 middle), while the sample with a nanocone array looked darkest (Fig. 11 right).

Absolute hemispherical measurements, collected with an integrating sphere, were used to quantitatively characterize these three samples (Fig. 12 above). The absorption over a wide range of wavelengths (400–800 nm) was measured. With the bandgap of a-Si:H around 1.75 eV, this range covers most of the useful spectral regime for a-Si:H solar cells. Between 400 and 650 nm, nanocone-array absorption was maintained above 93%, which was much better than for both the nanowire arrays (75%) and thin film (64%). The measured total absorption decreased to 88% at 700 nm – corresponding to the a-Si:H bandgap (1.75 eV) – which is also better than for either nanowires (70%) or thin film (53%).

Their total absorption for different angles of incidence is measured at a wavelength of 488 nm (Fig. 12 below). The sample with a nanocone array demonstrated the highest absorption, i.e., 98.4% around normal incidence, which offers a significant advantage over both nanowires (85%) and thin films (75%). The performance of the nanocone sample also showed a reduced dependence on the angle of incidence and significantly higher absorption at any angle. At angles of incidence up to 60°, the total absorption was maintained above 90%, which compares favorably with 70% and 45% for the nanowire array and thin film, respectively. Since all three samples start with 1 μm-thick, which is around the absorption depth of a-Si:H film, the absorption enhancement in the samples of nanowires and nanocones is believed to be mainly due to suppression of reflection from the front surface.

4. Photon management: absorption enhancement

Once light is coupled into solar cell devices with much reduced reflection, the next step of photon management is to increase the optical path length within the devices. For crystalline Si solar cells, a pyramid design, with features spanning tens of microns, can dramatically increase the optical path length of light with long wavelength. In geometrical optics, where dimensions are generally significantly larger than wavelengths, it is well known that absorption enhancement can be up to $4n^2/\sin^2\theta$, the Yablonovitch limit [29,30], with n as refractive index of the absorber layer, and θ as the angle of the emission cone in the medium surrounding the cell. However, for most of the next generation solar cell devices, the
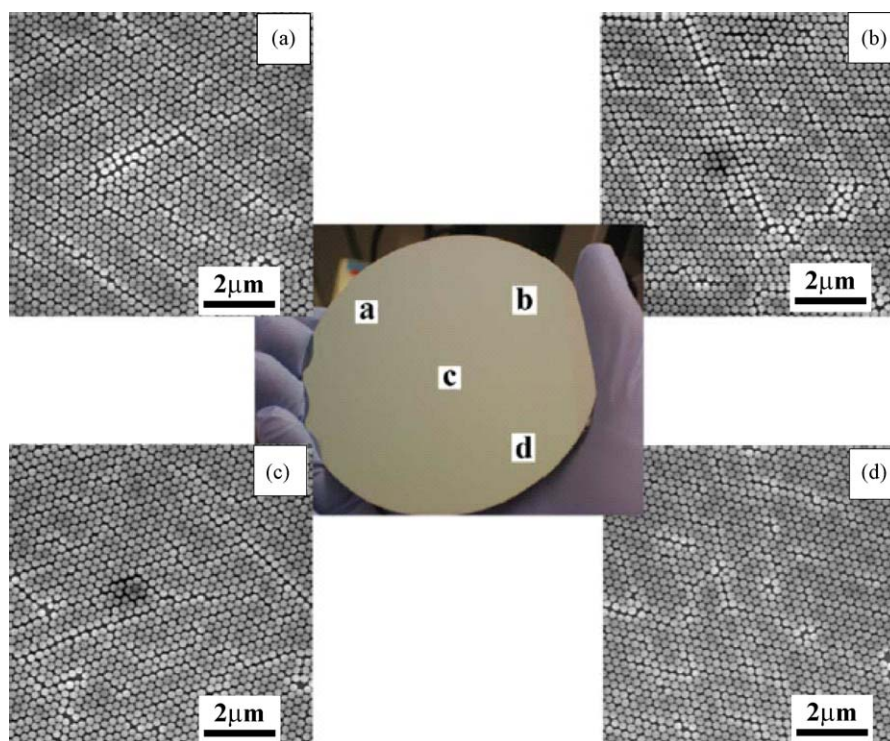
Fig. 7. A photograph of a 4-in. wafer with SiO$_2$ nanoparticle on the surface. (a)–(d) SEM images of four random spots with a uniform monolayer of SiO$_2$ nanoparticles.
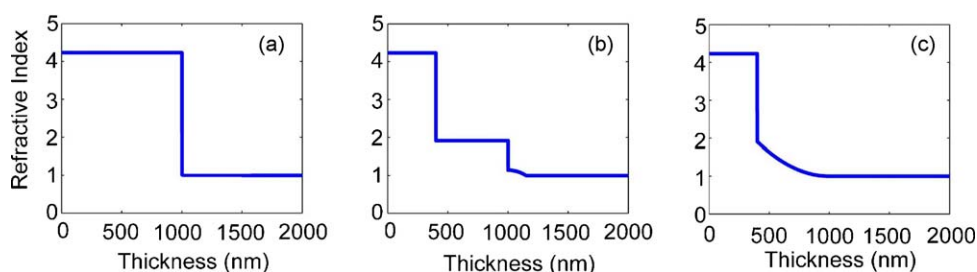

Fig. 8. The effective refractive index profiles of the interfaces between air and (a) a-Si:H thin film, (b) a-Si:H NW arrays, and (c) a-Si:H NC arrays.

thickness of the active layer is typically only around 1–2 μm, or less, which is comparable to the wavelengths of visible light. Increasing optical path length at the sub-wavelength regime calls for both a better physical understanding and novel process development.
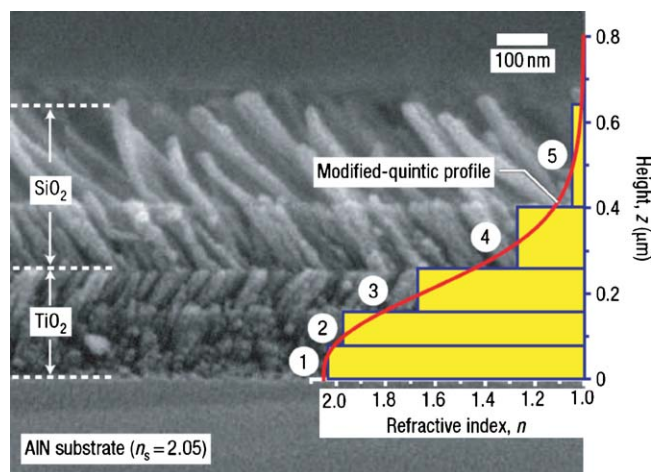

Fig. 9. (Ref. [27]) TiO$_2$–SiO$_2$ graded-index coating. Cross-sectional SEM image of graded-index coating with a modified-quintic-index profile. The graded-index coating consists of three TiO$_2$ nanorod layers and two SiO$_2$ nanorod layers.

4.1. Different mechanisms

Numerous ideas and designs have been proposed recently to use nanostructures for this purpose [31]. One notable example is plasmonic solar cells. Nanoparticles arrays of a noble metal, such as silver, have been incorporated for absorption enhancement in the region close to bandgap edge in a variety of devices. In those studies, the main mechanisms were believed to be the large resonant scattering cross-section of these particles or plasmonics. However, since these nanoparticles are on top of the surface, part of the short wavelength light around the resonant frequency is wasted by either scattering or absorption.

Photonic crystal designs based on well-defined nanostructure arrays are another highly pursued approach [32,33] (Fig. 13). However, the ultimate scales of practical application of those designs are determined by the scalability of techniques involved to achieve these photonic crystal structures.

4.2. Nanodome structures

Based on the fabrication process introduced in section II, we have demonstrated novel nanodome solar cells. They have periodic nanoscale modulation for all layers, from the bottom substrate, through the active absorber to the top transparent contact (Fig. 14). These devices combine many nanophotonic effects to both
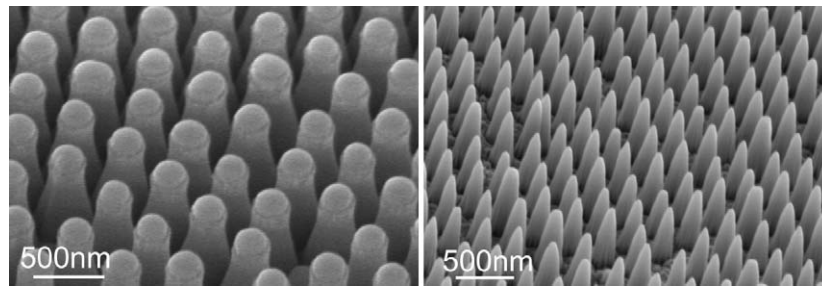
Fig. 10. SEM images of an a-Si:H nanowire array (left) and a nanocone array (right).
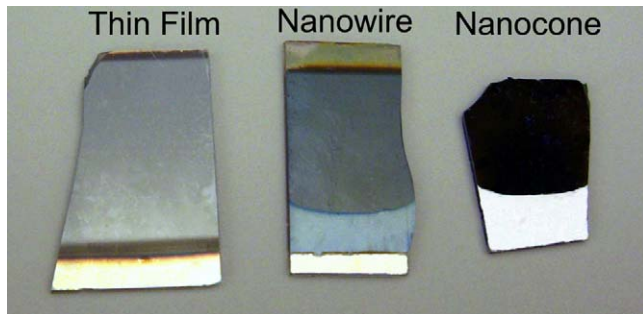

Fig. 11. (left) a-Si:H thin film, (middle) Nanowire arrays, and (right) nanocone arrays.

efficiently reduce reflection and enhance absorption over a broad spectral range.

We have chosen a-Si:H solar cells to demonstrate the advantages of the nanodome concept. As the second most produced solar cells, a-Si:H solar cells have several unique advantages. It is based on abundant, non-toxic materials, and can be fabricated by low temperature roll-to-toll processes (around 200 °C). More importantly, a-Si:H can absorb light efficiently, with an absorption depth of only 1 μm (at around 1.8 eV), several hundred times thinner than that of crystalline silicon. However, carriers of a-Si:H have poor transport properties, especially a short carrier diffusion length of around 300 nm. In addition, the 10–30% efficiency degradation under light soaking, known as the Stabler–Wronski effect, is found to be less severe with thinner films (below 300 nm). Hence, efficient light harvesting within a much thinner layer (<300 nm) is essential to the device performance of this type of solar cell.

The centerpiece of the nanodome structures is nanocone substrates (Fig. 15(a)). Nanocone glass or quartz substrates are

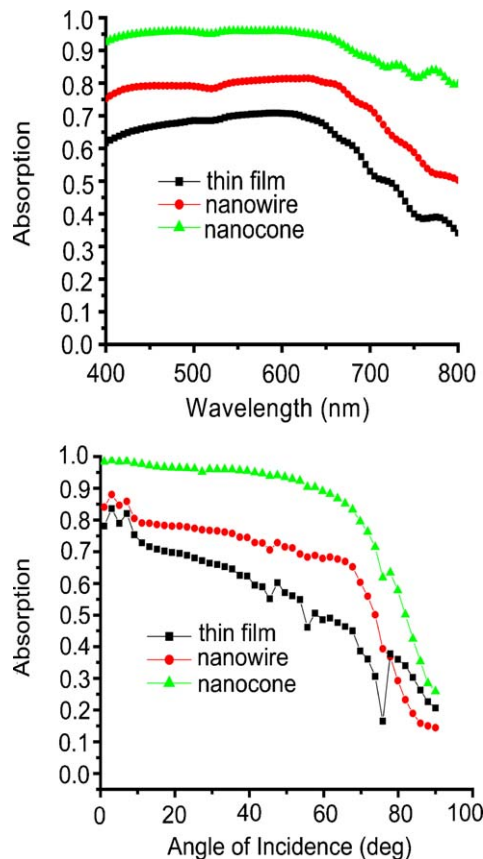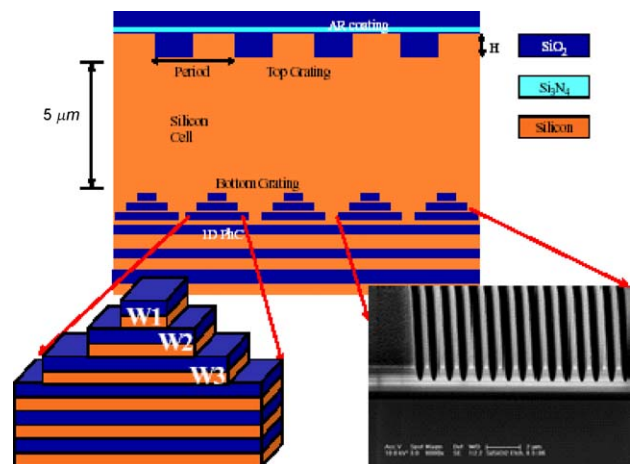Fig. 13. (Ref [32]) Schematic illustration of photonic crystal design based Solar Cells.

Fig. 12. Hemispherical absorption measurement on samples with a-Si:H thin film, a nanowire array and a nanocone array as top layer: wavelength dependence (at normal incidence) (above) and angles of incidence dependence (at wavelength λ = 488 nm) (below).
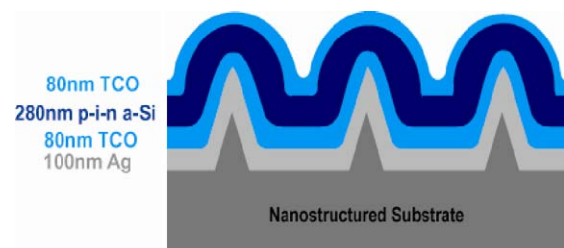

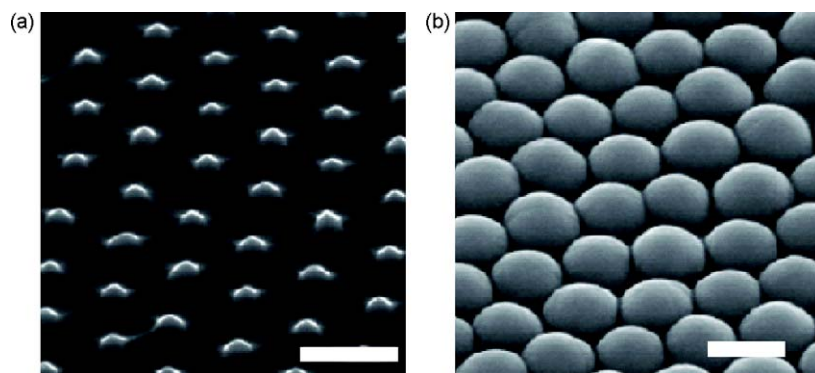Fig. 14. Schematic illustration of nanodome solar cells.

Fig. 15. Nanodome a-Si:H solar cell structure. SEM taken at 45° on (a) nanocone quartz substrate (b) a-Si:H nanodome solar cells after deposition of multilayers of materials on nanocones. Scale bar 500 nm.
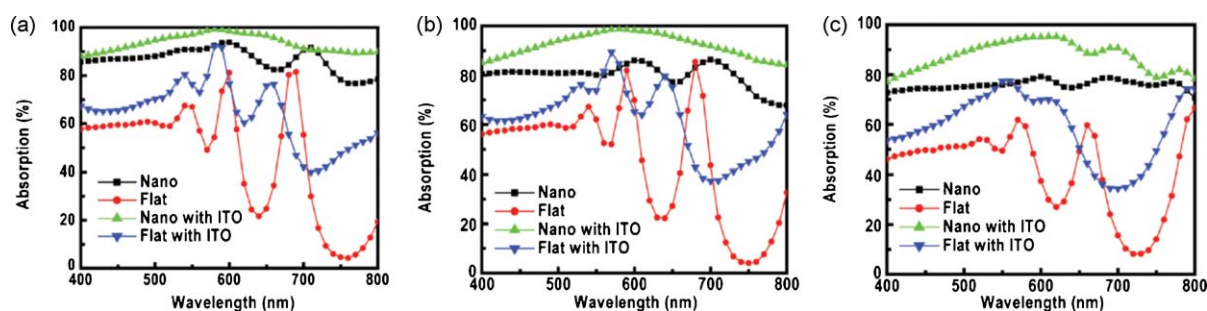

Fig. 16. Integrating sphere measurements of absorption under normal incidence (a), 30° angle of incidence (b), 60° angle of incidence (c). The samples are flat substrates without ITO coating (red), flat substrates with ITO coating (blue), nanodomes without ITO coating (black), and nanodomes with ITO coating (green) (For interpretation of the references to color in this figure legend, the reader is referred to the web version of the article.).

fabricated by Langmuir–Blodgett assembly of close-packed mono-disperse SiO_2 nanoparticles followed by reactive ion etching, as described in section II. The base diameters and spacings of nanocones can be controlled in the range of 100–1000 nm, which is relevant to wavelengths in the solar spectrum (Fig. 15(a)). A typical single p–i–n junction nanodome a-Si:H solar cell is conformally deposited on top of the nanocone substrates. The solar cell layers consist of 100 nm thick Ag as a back reflector, 80 nm thick transparent conducting oxide (TCO) as both bottom and top electrode, and a thin a-Si:H active layer of 280 nm (from top to bottom: p–i–n, 10–250–20 nm). After deposition, the nanocone pattern is largely transferred to the top layer, although nanocones become nanodomes, as shown in scanning electron microscopy (SEM) images (Fig. 15(b)).

The unique characteristic of this nanodome structure is that it has periodic nanoscale modulation for all layers, due to the nanostructured bottom layer. Because of this novel geometry, the nanodome solar cells have both anti-reflection and light-trapping effects. The results of the hemispherical absorption measurement on these nanodome solar cells are a clear indication of both of these two effects. We have measured absorption over a broad wavelength range (400–800 nm), which covers most of the spectrum that is useful for a-Si:H, which has a bandgap of 1.75 eV (or ~710 nm) (note: a-Si:H has a long band tail). For comparison, flat a-Si:H film solar cells with the same device structure and layer thickness were also measured. Since TCO has a lower refractive index (2.2) than that of a-Si:H (~4.23), measurements were carried out with and without the top TCO layer for both types of solar cells. The absorption data in the wavelength range of 400–800 nm under normal incidence are summarized in Fig. 16a. Green and black curves are from nanodome devices with and without the top TCO layers while blue and red ones are from flat film devices with and without the top TCO layers, respectively.

As shown in Fig. 16a, over the whole spectrum, nanodome devices show significantly larger absorption than flat film devices

with and without top ITO layers. The weighted absorption, integrated over the whole spectrum under the 1 Sun AM 1.5 illumination condition, is plotted in Fig. 17. Nanodomes with a top TCO layer show extremely high total weighted absorption of 94%, significantly higher than 65% achieved in flat films with a top TCO layer (Fig. 17).

As shown in Fig. 17, the absorption of nanodome and flat film devices with a top TCO layer is better than those without a top TCO layer, respectively. This is because TCO has a lower refractive index than a-Si:H so that light reflection is lower for the samples with the top TCO layers. However, this TCO enhancement effect is much less for nanodome devices (from 87% to 94%) than for flat film devices (from 48% to 65%), which indicates that the nanodome geometry without TCO already has very good anti-reflection property compared to the flat film geometry.
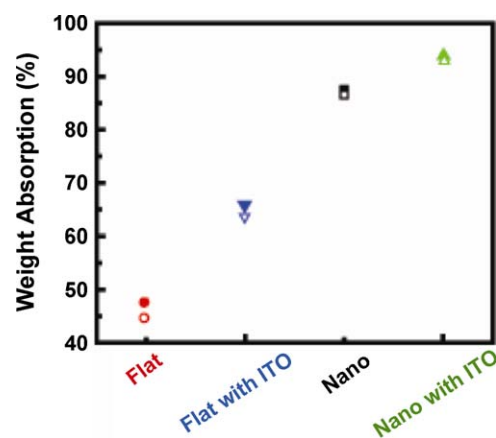

Fig. 17. The weighted absorption integrated over the wavelengths of 400–800 nm by experiment (solid symbols) and simulation (hollow symbols).
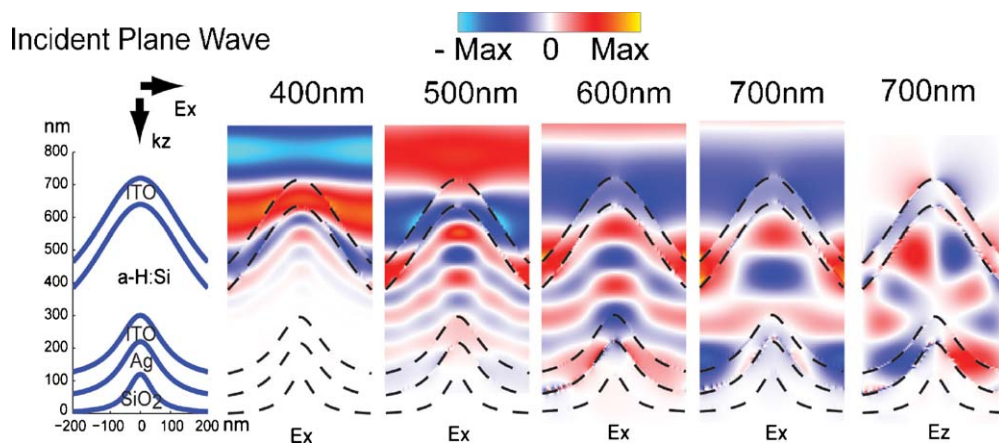
Fig. 18. Snapshots of simulated electric fields in the structure for different wavelengths.

The absorption enhancement comes from both suppressing reflection and increasing optical path length. While it is difficult to separate the two effects, since they are essentially coupled together, the anti-reflection effect is more dramatic in short wavelength region. In the case of a-Si:H solar cells, for the wavelength region below 500 nm, all the light loss can be attributed to the light reflection since its absorption depth (∼100 nm) is smaller than the a-Si:H layer thickness of 280 nm. As seen in Fig. 16(a), without the top TCO coating, the absorption of nanodomes is always above 85%, while the flat one is below 60%. Adding the TCO coating improves the absorption above 88% and 65% correspondingly. The anti-reflection effect is due to the tapered shape of nanodome structures, which provides better effective refractive index matching with air, similar to the nanocone case explained in Section 3.

The effect of increased optical path length plays a major role in the longer wavelength, where light is less efficiently absorbed. In the case of a-Si:H flat films, for the wavelengths above 550 nm, significant interference oscillations appear in flat film devices. However, nanodome devices still show relatively flat broadband adsorption (Fig. 16(a)). The observed oscillations in flat film devices are Fabry–Perot interference, arising from the long wavelength light not absorbed by the a-Si:H layer interfering with the reflected light from the top layer of the device. The interference oscillations are greatly reduced for the nanodome devices, suggesting that very little light escapes after reflection by the Ag. Their absence suggests significant light-trapping effects. The most interesting and significant absorption improvement using the nanodome geometry versus the flat film is in the wavelength range of 700–800 nm. a-Si:H has a bandgap of ∼710 nm and a long band tail. The absorption coefficient drops quickly when the light wavelength is above ∼700 nm. For flat film devices with the top TCO layer, there is a significant reduction of absorption down to 50% while nanodome devices with the top TCO layer maintain absorption of ∼90. These data suggest that nanodomes can enhance light trapping significantly even for the absorption of photons below the bandgap. However, it is hard to conclude at this moment whether any of the absorption in this wavelength range contributes to short-circuit current.

The dramatically increased optical path length in nanodome structures is due to the underlying nanoscale modulation of the Ag layer, which can couple light along the in-plane dimension, providing a light-trapping mechanism. Compared to the design of plasmonic solar cells, the nanostructured Ag back reflector as bottom contact in our nanodome devices is a better choice: while long wavelength light is strongly scattered by the modulated Ag back reflector, short wavelength absorption is not compromised

since significant absorption occurs during a single pass through the absorber, before reaching the Ag films. Compared with the Lambertian scattering, which is based on well-understood surface texturing using features much larger than light wavelengths for absorption enhancement, our devices use sub-wavelength nanodome structures, which are more feasible for solar cells with only sub-micrometer thick absorber layers.

The physical mechanisms of absorption enhancement are further elucidated by solving the Maxwell equations with three-dimensional finite-difference time-domain simulation on the experimental device geometry. The cross-section of the structure is shown in Fig. 18 (left) with incident plane waves polarized in the x direction. The period of the nanodome array is 450 nm. The dielectric constants of silver and silicon are taken from tabulated experimental data modeled by complex-conjugate pole-residue method. The simulated nanodome structure can absorb 93% of normally incident sunlight for the spectral range from 400 to 800 nm (Fig. 17 green triangle), which matches well with experimental data. The broadband absorption comes from two contributions. First, the reflection is greatly suppressed by the nanodomes. The dome shape forms a graded-refractive index profile, creating a broadband anti-reflection layer. For short wavelength around 400–500 nm (Fig. 18, Ex simulation for 400 and 500 nm), a-Si:H is highly absorptive. Thus, with efficient anti-reflection effects, all the incident lights are absorbed during a single path through the a-Si:H layer. Second, the nanodome shape can also efficiently couple the incident light into modes that are guided into the a-Si:H layer. (*Note*: The dispersion relation of such
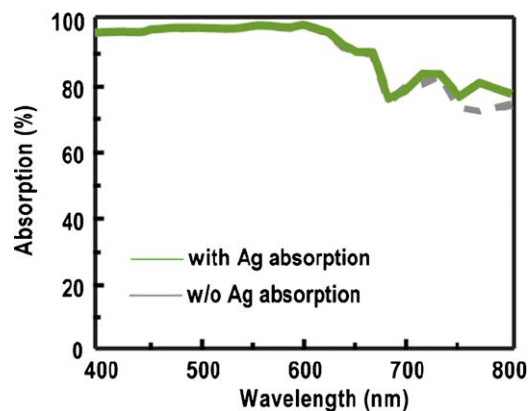

Fig. 19. Simulation of absorption spectra for the case with (green) and without (dashed grey) Ag absorption loss.
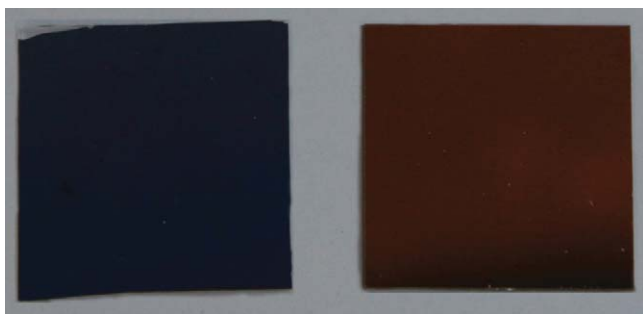
Fig. 20. Photographs of nanodome solar cells (left) and flat film solar cells (right).

modes can be strongly influenced by the presence of plasmonic responses of the Ag film.) This is particularly important for the long wavelength regime (Fig. 18, Ex simulation for 600 and 700 nm) where a-Si:H is less absorptive and all the incident light cannot be absorbed efficiently during a single path. In Fig. 17, the 'simulation for 700 nm shows the *z* component of the electric field, indicating strong guided modes confined inside the nanodome structure. Fig. 19 shows the absorption spectra with (green line) and without (grey line) metal loss, to evaluate the absorption loss by silver. For the lossless silver case, the weighted absorption for normal incident sunlight is 92% as compared to 93% for the realistic silver case. Therefore, the metal loss contributes only a negligible portion of absorption, which provides another advantage compared to plasmonic solar cells.

It is also very important to evaluate the absorption efficiency over a wide range of incident angles, since sun light can be quite diffuse in a practical environment. Fig. 16(b) and (c) shows the absorption measurement at incident angles of 30° and 60°, respectively. As the incident angle increases from 0° to 60°, the absorption over the whole spectrum decreases only by 5% for nanodome devices, while flat devices' absorption decreases by 13%. These data suggest that nanodome devices have an advantage over flat film devices in the real environment. Indeed, nanodome and flat film devices look very different even to the eye. Fig. 20(a) shows photographs of nanodomes (left) and flat films (right) without the top TCO layers in diffuse light conditions, respectively. The flat film devices are mirror-like, highly reflective, and look red because of inefficient light absorption at long wavelengths. However, nanodome devices look black due to efficient anti-reflection and light trapping.

5. Solar cell performance

Combining superior anti-reflection and efficient absorption enhancement, nanodome solar cell devices based on this novel

photon management design can achieve near perfect light absorption with thin active layers. Therefore, significant improvements in short-circuit current and efficiency can be achieved, compared to conventional devices (Fig. 21).

To prove how effectively anti-reflection and light trapping can improve the power conversion efficiency of solar cells, we have tested nanodome and flat film solar cell devices in a solar simulator with 1 sun AM1.5G illumination. Excitingly, the nanodome devices show power conversion efficiencies that are 25% higher than the flat film devices, made under otherwise identical conditions. An example is shown in Fig. 3(b), in which the nanodome device exhibits a power efficiency of 5.9% (open circuit voltage, V_{oc} = 0.75 V; short-circuit current, J_{sc} = 17.5 mA/cm^2; fill factor, FF = 0.45) while the flat device exhibits an efficiency of 4.7% (V_{oc} = 0.76 V, J_{sc} = 11.4 mA/cm^2, FF = 0.54). The significant improvement in power efficiency comes from the large short-circuit current of nanodome devices (17.5 mA/cm^2), which is higher than that (15.6 mA/cm^2) of the world record single junction a-Si:H solar cells with substrate configuration [22], with initial power efficiency of 10.6%. The short-circuit current of nanodome devices is only slightly lower than the theoretical value (20.5 mA/cm^2) limited by the bandgap. It is expected that the efficiency of nanodome devices can be further improved by improving the open circuit voltage and fill factor, via better materials deposition.

6. Summary and outlook

Advanced photon management is essential for the development of next generation photovoltaic devices, to achieve higher efficiency, lower cost and finally enable terawatt-scale applications. Nanostructures with unique scales and geometries are destined to play a critical role in the photon management in the sub-wavelength regime. Even though the rapidly evolving field of nanotechnology has provided a variety of tools to tailor nanostructures, broadband coverage of the solar spectrum and strict cost limitation of solar cell modules make the task of efficient photon management rather challenging.

We have designed a novel nanodome structure which can efficiently suppress reflection while simultaneously enhancing absorption. The center piece of this nanodome structure is the nanocone template, which can be achieved through a low temperature, large-scale process. The nanodome design is not limited to specific materials, and the shapes, diameters, and spacings of nanocone templates can be tailored precisely across a wide range for different types of solar cells. The a-Si:H nanodome solar cells that we used for this demonstration of concept can achieve efficiencies 25% higher than that of flat film control. We have also proved that in the sub-wavelength regime, light-trapping can greatly enhance absorption.
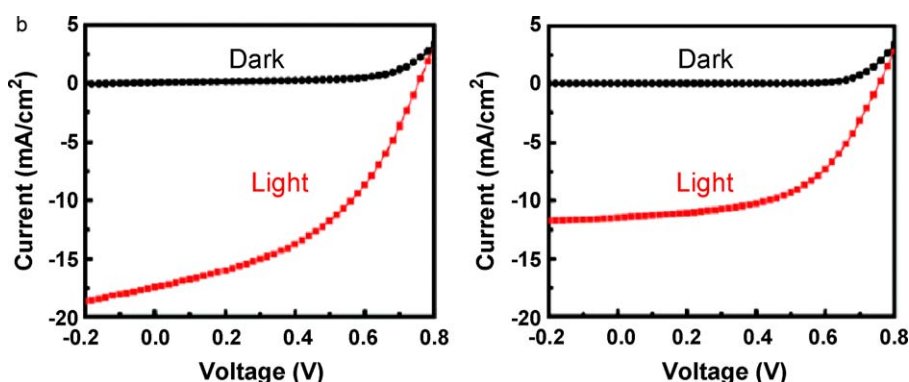

Fig. 21. Dark and light *I–V* curve of solar cell devices for nanodomes (left) and flat substrates (right).

An effective integration of fundamental mechanistic understanding and novel processing development is the key to the efficient photon manipulations for solar cell applications. Every step in each of these two domains will ultimately lead to the success of the development of next generation solar cells, and may well spawn many other unexpected scientific discoveries and technological applications.

References

[1] A.V. Shah, H. Schade, M. Vanecek, J. Meier, E. Vallat-Sauvain, N. Wyrsch, U. Kroll, C. Droz, J. Bailat, Progress in Photovoltaics 12 (2–3) (2004) 113–142.
[2] D.E. Carlson, C.R. Wronski, Applied Physics Letters 28 (11) (1976) 671–673.
[3] R.A. Street, Hydrogenated Amorphous Silicon, Cambridge University Press, 1991.
[4] J. Zhao, A. Wang, P.P. Altermatt, S.R. Wenham, M.A. Green, Solar Energy Materials Solar Cells 41/42 (1996) 87.
[5] N. Engheta, Science 317 (5845) (2007) 1698–1702.
[6] T.W. Ebbesen, H.J. Lezec, H.F. Ghaemi, T. Thio, P.A. Wolff, Nature 391 (6668) (1998) 667–669.
[7] E. Ozbay, Science 311 (5758) (2006) 189–193.
[8] W.L. Barnes, A. Dereux, T.W. Ebbesen, Nature 424 (6950) (2003) 824–830.
[9] P.R. Barry, P. Peter, R.F. Stephen, Journal of Applied Physics 96 (12) (2004) 7519–7526.
[10] K.R. Catchpole, A. Polman, Optics Express 16 (26) (2008) 21793–21800.
[11] K.R. Catchpole, A. Polman, Applied Physics Letters 93 (19) (2008) 191113.
[12] D. Derkacs, S.H. Lim, P. Matheu, W. Mar, E.T. Yu, Applied Physics Letters 89 (9) (2006) 093103.
[13] V.E. Ferry, L.A. Sweatlock, D. Pacifici, H.A. Atwater, Nano Letters 8 (12) (2008) 4391–4397.
[14] N. Keisuke, T. Katsuaki, A.A. Harry, Applied Physics Letters 93 (12) (2008) 121904.
[15] S. Pillai, K.R. Catchpole, T. Trupke, M.A. Green, Journal of Applied Physics 101 (9) (2007) 093105.
[16] L. Christy, R.P.V.D. Haynes, The Journal of Physical Chemistry B 24 (2001) 5599.
[17] A. Kosiorek, W. Kandulski, P. Chudzinski, K. Kempa, M. Giersig, Nano Letters 4 (7) (2004) 1359.
[18] C.-M. Hsu, S.T. Conor, M.X. Tang, Y. Cui, Applied Physics Letters 93 (13) (2008) 133109.
[19] J. Zhu, Z. Yu, G.F. Burkhard, C.-M. Hsu, S.T. Connor, Y. Xu, Q. Wang, M. McGehee, S. Fan, Y. Cui, Nano Letters 9 (1) (2009) 279–282.
[20] T. Fujii, Y. Gao, R. Sharma, E.L. Hu, S.P. DenBaars, S. Nakamura, Applied Physics Letters 84 (6) (2004) 855–857.
[21] E.F. Schubert, Light Emitting Diodes, 2nd edn., Cambridge University Press, Cambridge, UK, 2006.
[22] H. Kim, K.K. Choi, K.K. Kim, J. Cho, S.N. Lee, Y. Park, J.S. Kwak, T.Y. Seong, Optics Letters 33 (11) (2008) 1273–1275.
[23] L. Hu, G. Chen, Nano Letters 7 (11) (2007) 3249–3252.
[24] B.J.P.J. Wei-Lun Min, Advanced Materials 9999 (9999) (2008), NA.
[25] T. Lohmuller, M. Helgert, M. Sundermann, R. Brunner, J.P. Spatz, Nano Letters 8 (5) (2008) 1429–1433.
[26] Y.J. Lee, D.S. Ruby, D.W. Peters, B.B. McKenzie, J.W.P. Hsu, Nano Letters 8 (5) (2008) 1501–1505.
[27] J.Q. Xi, M.F. Schubert, J.K. Kim, E.F. Schubert, M. Chen, S.-Y. Lin, LiuW, J.A. Smart, Nature Photonics 1 (3) (2007) 176–179.
[28] Y.-F. Huang, S. Chattopadhyay, Y.-J. Jen, C.-Y. Peng, T.-A. Liu, Y.-K. Hsu, C.-L. Pan, H.-C. Lo, C.-H. Hsu, Y.-H. Chang, C.-S. Lee, K.-H. Chen, L.-C. Chen, Nature Nanotechnology 2 (12) (2007) 770–774.
[29] T. Tiedje, E. Yablonovitch, G.D. Cody, B.G. Brooks, IEEE Transactions on Electron Devices 31 (5) (1984) 711–716.
[30] E. Yablonovitch, Journal of Optical Society of America 72 (7) (1982) 899–907.
[31] O.L. Muskens, J.G. Rivas, R.E. Algra, E.P.A.M. Bakkers, A. Lagendijk, Nano Letters 8 (9) (2008) 2638–2642.
[32] J.G. Mutitu, S. Shi, C. Chen, T. Creazzo, A. Barnett, C. Honsberg, D.W. Prather, Optics Express 16 (19) (2008) 15238–15248.
[33] M.J. Hampton, S.S. Williams, Z. Zhou, J. Nunes, D. Ko, J.L. Templeton, E.T. Samulski, J.M. DeSimone, Advanced Materials 20 (14) (2008) 2667.
[34] R. Noufi, K. Zweibel, IEEE 4th World Conference on Photovoltaic Energy Conversion (WCPEC-4) Waikoloa, Hawaii (May 7-12, 2006) 2006.